Supporting Information for "The 2019-2020 Australian drought and bushfires altered the partitioning of hydrological fluxes"

Sujay V. Kumar

Hydrological Sciences Laboratory, NASA GSFC, Greenbelt, MD

Thomas Holmes

Hydrological Sciences Laboratory, NASA GSFC, Greenbelt, MD

Niels Andela

School of Earth and Ocean Sciences, Cardiff University, Cardiff, UK

Imtiaz Dharssi

Bureau of Meteorology, Melbourne, Australia,

Bushfire and Natural Hazard Cooperative Research Centre, Melbourne, Australia

Vinodkumar

Bureau of Meteorology, Melbourne, Australia,

Bushfire and Natural Hazard Cooperative Research Centre, Melbourne, Australia

Christopher Hain

Short-term Prediction Research and Transition Center, NASA MSFC, Huntsville, AL

Christa Peters-Lidard

Earth Science Division, NASA GSFC, Greenbelt, MD

Sarith P. Mahanama

Science Systems and Applications Inc, Lanham, MD

Global Modeling and Assimilation Office, NASA GSFC, Greenbelt, MD

Kristi R. Arsenault

Science Applications International Corporation, McLean, VA

Hydrological Sciences Laboratory, NASA GSFC, Greenbelt, MD

Wanshu Nie

Department of Earth and Planetary Sciences, Johns Hopkins University, Baltimore, MD

NASA Goddard Earth Sciences Technology and Research (GESTAR), Greenbelt, MD

Augusto Getirana

Science Applications International Corporation, McLean, VA

Hydrological Sciences Laboratory, NASA GSFC, Greenbelt, MD

Contents of this file

Introduction

Text S1: Details of the modeling and data assimilation configurations

The model configuration employs the modified International Geosphere Biosphere Programme (IGBP) MODIS 20 category landcover data (*Friedl et al.* [2002]), soil parameters derived from the International Soil Reference and Information Centre (ISRIC; *Hengl et al.* [2014]), and the Shuttle Radar Topography Mission (SRTM; *Rodriguez et al.* [2005]) based elevation, slope, and aspect data. Statistical downscaling approaches are used to transform the coarse resolution MERRA2 meteorological inputs to 1km. The input meteorological fields of air temperature, humidity, surface pressure, wind,

Sujay V. Kumar, Hydrological Sciences Laboratory, NASA Goddard Space Flight Center, Greenbelt, MD 20771. email: Sujay.V.Kumar@nasa.gov

downward shortwave radiation, and downward longwave radiation are downscaled to 1km by adjusting for terrain differences in elevation, slope, and aspect (*Kumar et al.* [2013]). The high resolution monthly precipitation climatology from WorldClim (*Fick and Hijmans* [2017]) is used to spatially disaggregate input MERRA2 precipitation to 1km. The initial conditions for the model simulations are generated from a long spinup of NoahMP starting from year 2000. All model integrations and evaluations are conducted using the NASA Land Information System (LIS; *Kumar et al.* [2006]) and the Land surface Verification Toolkit (LVT; *Kumar et al.* [2012]).

The data assimilation integrations employ a 1-dimensional Ensemble Kalman Filter (EnKF), which allows the update and propagation of a selected set of model states based on the observational information. The assimilation update at time k is represented as:

$$x_k^{i+} = x_k^{i-} + \mathbf{K}_k \left[y_k^i - \mathbf{H}_k x_k^{i-} \right], \tag{1}$$

where x_k^{i-} and x_k^{i+} represents the model state for the i^{th} ensemble member before and after the update, respectively. The observation operator $\mathbf{H}_k$ connects the model states to the observation space. The Kalman gain term ($\mathbf{K}_k$), computed based on the model and observation error covariances, provides the weighting factor between the model states and the observations.

In the assimilation configurations for VOD and LAI, ensemble spread is created by applying small perturbations to a number of meteorological forcing inputs (downward shortwave radiation, downward shortwave radiation, and precipitation) and the modeled LAI states, at each grid point. Multiplicative perturbations with a mean of 1 and standard deviations of 0.3 and 0.5, respectively, are applied to the precipitation (P) and downward shortwave (SW) fields. The longwave radiation field (LW) is perturbed with zero-mean, normally distributed additive perturbations with a standard deviation of 50 W/m^2. Time series correlations are imposed via a first-order regressive model (AR(1)) with a timescale of 24 hours. These perturbations also include cross correlations (ρ) between the forcing fields ($\rho(SW,P)$ = -0.8, $\rho(SW,LW)$ = -0.5, $\rho(LW,P)$ = 0.5). These perturbations are developed based on prior studies *Kumar et al.* [2019, 2020] and are applied at an hourly frequency. The model state vector in both VOD and LAI assimilation configurations consists of the prognostic LAI variable in NoahMP. Additive perturbations with a standard deviation of 0.01 are applied to the model state vector. The assimilation configurations also directly update the leaf biomass within NoahMP by dividing the LAI with the specific leaf area, consistent with the Noah-MP physics formulation *Liu et al.* [2016]. A uniform input observation error standard deviation of 0.05 for the scaled VOD retrievals and MODIS LAI is employed here, based on the settings established in previous studies *Kumar et al.* [2019, 2020].

In the VOD DA configuration, the SMAP retrievals are rescaled into the LAI space using a seasonally varying CDF-matching approach (*Kumar et al.* [2015]) using the MODIS LAI observations from the Global Land Cover Facility (GLCF) LAnd Surface Satellites (GLASS; *Xiao et al.* [2016]) project at the University of Maryland. This rescaling is performed as prior studies (*Konings et al.* [2017]; *Albergel et al.* [2018]) have established the strong correlation between VOD and vegetation indices such as LAI. The

SMAP VOD CDFs are computed using a time period of 2015 to 2020, whereas the MODIS LAI CDFs are computed across 2000-2018, which is the available time period of the GLASS LAI data. Since SMAP data is only available for a period of approximately 5 years, we use a spatial sampling window of 2 pixels to increase the sampling density of seasonal CDF calculations. The assimilation integrations are conducted in a sequential manner, based on the local overpass time of the SMAP measurements.

Text S2: Description of the SMAP VOD dataset

SMAP (*Entekhabi et al.* [2010]) is a mission that employs an L-band radiometer to measure soil moisture. The soil moisture and VOD products from SMAP are derived through the retrieval approach that employs the first-order τ-ω radiative transfer model (*Mo et al.* [1982]). The τ-ω model estimates the top of the atmosphere brightness temperatures in the L-band as a function of the surface soil temperature, canopy temperature, and surface reflectivity. In this study, we use the level 2 SMAP dataset (SPL2SMP_E), which provides soil moisture and VOD retrievals at 9km spatial resolution through Backus-Gilbert interpolation applied to oversampled antenna measurements. This particular SMAP retrieval is obtained from the Modified Dual Channel Algorithm (MDCA; *Chaubell et al.* [2016]), which employs both the vertically and horizontally polarized brightness temperature observations to derive vegetation optical depth.

Text S3: Description of the MODIS LAI dataset

The MCD15A2H collection 6 LAI data (*R. Myneni* [2015]), which provides LAI estimates at 500m spatial resolution at 8-day intervals from the MODIS sensors located on

NASA's Terra and Aqua satellites, is used for LAI DA integrations. The relationship between MODIS reflectance observations and canopy structure is exploited for developing these LAI estimates. The 500m resolution data is aggregated to the 1km model resolution within the DA integrations. In addition, only data values that are designated as 'good quality', which considers factors such as cloud contamination, detector signal quality, algorithm saturation issues (*Myneni et al.* [2002]), are used in the assimilation integrations.

Text S4: Description of evaluation datasets

The Atmosphere-Land Exchange Inverse (ALEXI; *Anderson et al.* [2007])) data employs MODIS thermal infrared (TIR) measurements as the main diagnostic (*Hain and Anderson* [2017]) to develop daily gridded estimates of ET. In this article, we also use the in-situ eddy-covariance ET measurements from the OzFlux network (http://www.ozflux.org.au) over 9 locations in Eastern Australia (Figure S1). These locations are chosen based on the availability of data during the 2015 -2020 time period.

Streamflow data from 194 locations in southeast Australia from the Australian Bureau of Meteorology's Hydrologic Reference Stations (HRS) network is used for runoff evaluations. Using the quality control information provided in the data, only measurements that are characterized as 'good quality' are employed in the evaluations. As noted in the HRS documentation, these sites represent locations largely unaffected by water management impacts such as reservoir operations.

The Australian Bureau of Meteorology's high resolution soil moisture analysis called JASMIN (Joint UK Land Environment Simulator (JULES)-based Soil Moisture Information; *Vinodkumar and Dharssi* [2019]) is a 5km resolution, land surface model-based soil moisture analysis driven by observed meteorology. Though JASMIN estimates are also model-derived, we use it as a reference data as prior studies have established reasonable skill in comparisons against ground measurements. 18 locations over NSW from the ISMN network with soil moisture profile measurements, are used in the ISMN evaluations (Figure S1).

Text S5: Description of evaluation metrics

The spatial similarity of the vegetation anomalies from SMAP and the burn scar features from MCD64A1 is estimated using the categorical measures of Accuracy and kappa-coefficient. Accuracy is estimated as:

$$\text{Accuracy} = \frac{\text{TP+TN}}{\text{TP+FP+FN+TN}} \tag{2}$$

where TP is the total number of true positives, TN the total number of true negatives, FP the number of false positives, and FN the number of false negatives. A true positive detection is assumed when a negative SMAP VOD anomaly below a value of -0.2 is coincident with a burn scar detection in the MCD64A1 data. Similarly, a true negative occurrence results when a positive VOD anomaly and no burn scar classification from MCD64A1 at a location is obtained. The false positive cases are obtained when a negative SMAP VOD anomaly is coincident with burn scar free classification from

MCD64A1. Conversely, when a positive SMAP VOD anomaly matches with a burn scar classification, a false negative case is assumed.

The kappa coefficient (K) is computed as the ratio of the observed agreement between two datasets relative to the expected level of agreement. K is expressed as:

$$\mathrm{K} = \frac{(p_o - p_e)}{(1 - p_e)} \tag{3}$$

where p_o is the same as Accuracy and p_e is calculated as:

$$p_e = \frac{\text{(TP+FN)*(TP+FP)+(FP+TN)*(FN+TN)}}{\text{(TP+FP+FN+TN)}^2} \tag{4}$$

The impact of DA on runoff was evaluated using the Normalized Information Contribution (NIC) metric, which is defined for correlation (R) and Nash Sutcliffe Efficiency (NSE) as follows:

$$\mathrm{NIC}_R = \frac{(R_a - R_o)}{(1 - R_o)} \tag{5}$$

$$\mathrm{NSE}_R = \frac{(\mathrm{NSE}_a - \mathrm{NSE}_o)}{(1 - \mathrm{NSE}_o)} \tag{6}$$

$$\tag{7}$$

where the subscripts a and o represent the DA and OL integrations, respectively. The NIC metric provides a measure of the skill improvement as a fraction of the maximum possible skill improvement. Positive NIC values indicate beneficial impacts from assimilation and negative values suggest degradations from DA relative to OL.

Figure S1: Map of the modeling domain

Figure S2: Impact of DA on soil moisture estimates

References

Albergel, C., S. Munier, A. Bocher, B. Bonan, Y. Zheng, C. Draper, D. Leroux, and J.-C. Calvet, LDAS-Monde sequential assimilation of satellite derived observations applied to the contiguous US: An ERA-5 driven reanalysis of the land surface variables, *Remote Sensing*, *10*(10), 1627, 2018.

Andela, N., Y. Y. Liu, A. I. J. M. van Dijk, R. A. M. de Jeu, and T. R. McVicar, Global changes in dryland vegetation dynamics (1988–2008) assessed by satellite remote sensing: comparing a new passive microwave vegetation density record with reflective greenness data, *Biogeosciences*, *10*(10), 6657–6676, doi:10.5194/bg-10-6657-2013, 2013.

Anderson, M., J. Norman, J. Mecikalski, J. Otkin, and W. Kustas, A climatological study of evapotranspiration and moisture stress across the continental U.S. based on thermal remote sensing: I. Model formulation, *Journal of Geophysical Research*, *112*(D10117), doi:10.1029/2006JD007506, 2007.

Boer, M., V. Resco de Dios, and R. Bradstock, Unprecedented burn area of Australian mega forest fires, *Nature Climate Change*, *10*, 171–172, doi:10.1038/s41558-020-0716-1, 2020.

Chaubell, J., S. Yueh, D. Entekhabi, and J. Peng, Resolution enhancement of smap radiometer data using the backus gilbert optimum interpolation technique, in *2016 IEEE International Geoscience and Remote Sensing Symposium (IGARSS)*, pp. 284–287, 2016.

Chow, V., *Applied Hydrology*, McGraw-Hill, NY, 1964.

Dorigo, W. A., et al., The International Soil Moisture Network: a data hosting facility for global in situ soil moisture measurements, *Hydrology and Earth System Sciences*, *15*(5), 1675–1698, doi:10.5194/hess-15-1675-2011, 2011.

Entekhabi, D., et al., The Soil Moisture Active Passive (SMAP) Mission, *Proceedings of the IEEE*, *98*(5), 704–716, doi:10.1109/jproc.2010.2043918, 2010.

Fick, S. E., and R. J. Hijmans, WorldClim 2: new 1-km spatial resolution climate surfaces for global land areas, *International Journal of Climatology*, *37*(12), 4302–4315, doi:10.1002/joc.5086, 2017.

Friedl, M., et al., Global land cover mapping from MODIS: algorithms and early results, *Remote Sensing of Environment*, *83*(1), 287 – 302, doi:https://doi.org/10.1016/S0034-4257(02)00078-0, 2002.

Gelaro, R., et al., The Modern-Era Retrospective Analysis for Research and Applications, Version 2 (MERRA-2), *Journal of Climate*, *30*(14), 5419–5454, doi:10.1175/JCLI-D-16-0758.1, 2017.

Giglio, L., L. Boschetti, D. P. Roy, M. L. Humber, and C. O. Justice, The collection 6 modis burned area mapping algorithm and product, *Remote Sensing of Environment*, *217*, 72 – 85, doi:https://doi.org/10.1016/j.rse.2018.08.005, 2018.

Hain, C. R., and M. C. Anderson, Estimating morning change in land surface temperature from MODIS day/night observations: Applications for surface energy balance modeling, *Geophysical Research Letters*, *44*(19), 9723–9733, doi:10.1002/2017GL074952, 2017.

Hajj, E., N. Baghdadi, J.-P. Wigneron, M. Zribi, C. Algergel, J.-C. Calvet, and I. Fayad, First Vegetation Optical Depth Mapping from Sentinel-1 C-band SAR Data over Crop Fields, *Remote Sensing*, *11*(23), 2769, 2019.

Hengl, T., et al., SoilGrids1km - Global Soil Information Based on Automated Mapping, *PLoS ONE*, *9*(8), doi:10.1371/journal.pone.0105992, 2014.

Houborg, R., J. B. Fisher, and A. K. Skidmore, Advances in remote sensing of vegetation function and traits, *International Journal of Applied Earth Observation and Geoinformation*, *43*, 1 – 6, doi:https://doi.org/10.1016/j.jag.2015.06.001, special Issue on ”Advances in remote sensing of vegetation function and traits”, 2015.

King, A., A. Pitman, B. Henley, A. Ukkola, and J. Brown, The role of climate variability in Australian drought, *Nature Climate Change*, *10*, 177–179, doi:10.1038/s41558-020-0718-z, 2020.

Konings, A. G., and P. Gentine, Global variations in ecosystem-scale isohydricity, *Global change biology*, *23*(2), 891–905, 2017.

Konings, A. G., M. Piles, N. Das, and D. Entekhabi, L-band vegetation optical depth and effective scattering albedo estimation from SMAP, *Remote Sensing of Environment*, *198*, 460 – 470, doi:https://doi.org/10.1016/j.rse.2017.06.037, 2017.

Kumar, S., C. Peters-Lidard, J. Santanello, K. Harrison, Y. Liu, and M. Shaw, Land surface Verification Toolkit (LVT) - a generalized framework for land surface model evaluation, *Geoscientific Model Development*, *5*, 869–886, doi:10.5194/gmd-5-869-a, 2012.

Kumar, S., et al., Land Information System: An interoperable framework for high resolution land surface modeling, *Environmental Modeling and Software*, *21*, 1402–1415, 2006.

Kumar, S. V., R. H. Reichle, R. D. Koster, W. T. Crow, and C. D. Peters-Lidard, Role of Subsurface Physics in the Assimilation of Surface Soil Moisture Observations, *Journal of Hydrometeorology*, *10*(6), 1534–1547, doi:10.1175/2009JHM1134.1, 2009.

Kumar, S. V., C. D. Peters-Lidard, D. Mocko, and T. Yudong, Multiscale Evaluation of the Improvements in Surface Snow Simulation through Terrain Adjustments to Radiation, *Journal of Hydrometeorology*, *14*(1), 220–232, doi:10.1175/JHM-D-12-046.1, 2013.

Kumar, S. V., C. D. Peters-Lidard, J. A. Santanello, R. H. Reichle, C. S. Draper, R. D. Koster, G. Nearing, and M. F. Jasinski, Evaluating the utility of satellite soil moisture retrievals over irrigated areas and the ability of land data assimilation methods to correct for unmodeled processes, *Hydrology and Earth System Sciences*, *19*(11), 4463–4478, doi:10.5194/hess-19-4463-2015, 2015.

Kumar, S. V., D. M. Mocko, S. Wang, C. D. Peters-Lidard, and J. Borak, Assimilation of Remotely Sensed Leaf Area Index into the Noah-MP Land Surface Model: Impacts on Water and Carbon Fluxes and States over the Continental United States, *Journal of Hydrometeorology*, *20*(7), 1359–1377, doi:10.1175/jhm-d-18-0237.1, 2019.

Kumar, S. V., T. R. Holmes, R. Bindlish, R. de Jeu, and C. Peters-Lidard, Assimilation of vegetation optical depth retrievals from passive microwave radiometry, *Hydrology and Earth System Sciences*, *24*(7), 3431–3450, doi:10.5194/hess-24-3431-2020, 2020.

Landis, J., and G. Koch, The measurement of observer agreement for categorical data, *Biometrics*, *33*(1), 159–174, 1977.

Liu, X., F. Chen, M. Barlage, G. Zhou, and D. Niyogi, Noah-MP-Crop: Introducing dynamic crop growth in the Noah-MP land surface model, *Journal of Geophysical Research: Atmospheres*, *121*(23), 13,953–13,972, doi:10.1002/2016JD025597, 2016.

Meesters, A. G. C. A., R. A. M. De Jeu, and M. Owe, Analytical derivation of the vegetation optical depth from the microwave polarization difference index, *IEEE Geoscience and Remote Sensing Letters*, *2*(2), 121–123, doi:10.1109/LGRS.2005.843983, 2005.

Mo, T., B. J. Choudhury, T. J. Schmugge, J. R. Wang, and T. J. Jackson, A model for microwave emission from vegetation-covered fields, *Journal of Geophysical Research: Oceans*, *87*(C13), 11,229–11,237, doi:10.1029/JC087iC13p11229, 1982.

Myneni, R., et al., Global products of vegetation leaf area and fraction absorbed PAR from year one of MODIS data, *Remote Sensing of Environment*, *83*(1), 214 – 231, doi: https://doi.org/10.1016/S0034-4257(02)00074-3, the Moderate Resolution Imaging Spectroradiometer (MODIS): a new generation of Land Surface Monitoring, 2002.

Niu, G.-Y., et al., The community Noah land surface model with multiparameterization options (Noah-MP): 1. Model description and evaluation with local-scale measurements, *Journal of Geophysical Research: Atmospheres*, *116*(D12109), doi:10.1029/2010JD015139, 2011.

Njoku, E. G., and D. Entekhabi, Passive microwave remote sensing of soil moisture, *Journal of Hydrology*, *184*(1), 101 – 129, doi:https://doi.org/10.1016/0022-1694(95)02970-2, soil Moisture Theories and Observations, 1996.

Pitman, A., G. Narisma, and J. McAneney, The impact of climate change on the risk of forest and grassland fires in Australia, *Climate Change*, *84*, 383–401, doi:10.1007/

s10584-007-9243-6, 2007.

R. Myneni, Y. K., MCD15A2H MODIS/Terra+Aqua Leaf Area Index/FPAR 8-day L4 Global 500m SIN Grid V006, doi:10.5067/MODIS/MCD15A2H.006, 2015.

Rodriguez, E., C. Morris, J. Belz, E. Chapin, J. Martin, W. Daffer, and S. Hensley, An assessment of the SRTM topographic products, *Tech. Rep. JPL D-31639*, Jet Propulsion Laboratory, Pasadena, CA, 2005.

van Marle, M. J. E., G. R. van der Werf, R. A. M. de Jeu, and Y. Y. Liu, Annual South American forest loss estimates based on passive microwave remote sensing (1990–2010), *Biogeosciences*, *13*(2), 609–624, doi:10.5194/bg-13-609-2016, 2016.

Vinodkumar, and I. Dharssi, Evaluation of daily soil moisture deficit used in Australian forest fire danger rating sytem, *Tech. Rep. 022*, Bureau of Meteorology, 2017.

Vinodkumar, and I. Dharssi, Evaluation and calibration of a high-resolution soil moisture product for wildfire prediction and management, *Agricultural and Forest Meteorology*, *264*, 27 – 39, doi:https://doi.org/10.1016/j.agrformet.2018.09.012, 2019.

Xiao, Z., S. Liang, J. Wang, Y. Xiang, X. Zhao, and J. Song, Long-Time-Series Global Land Surface Satellite Leaf Area Index Product Derived From MODIS and AVHRR Surface Reflectance, *IEEE Transactions on Geoscience and Remote Sensing*, *54*(9), 5301–5318, doi:10.1109/TGRS.2016.2560522, 2016.

Yang, G.-Y., Z.-L.and Niu, et al., The community Noah land surface model with multiparameterization options (Noah-MP): 2. Evaluation over global river basins, *Journal of Geophysical Research: Atmospheres*, *116*(D12), doi:10.1029/2010JD015140, d12110, 2011.

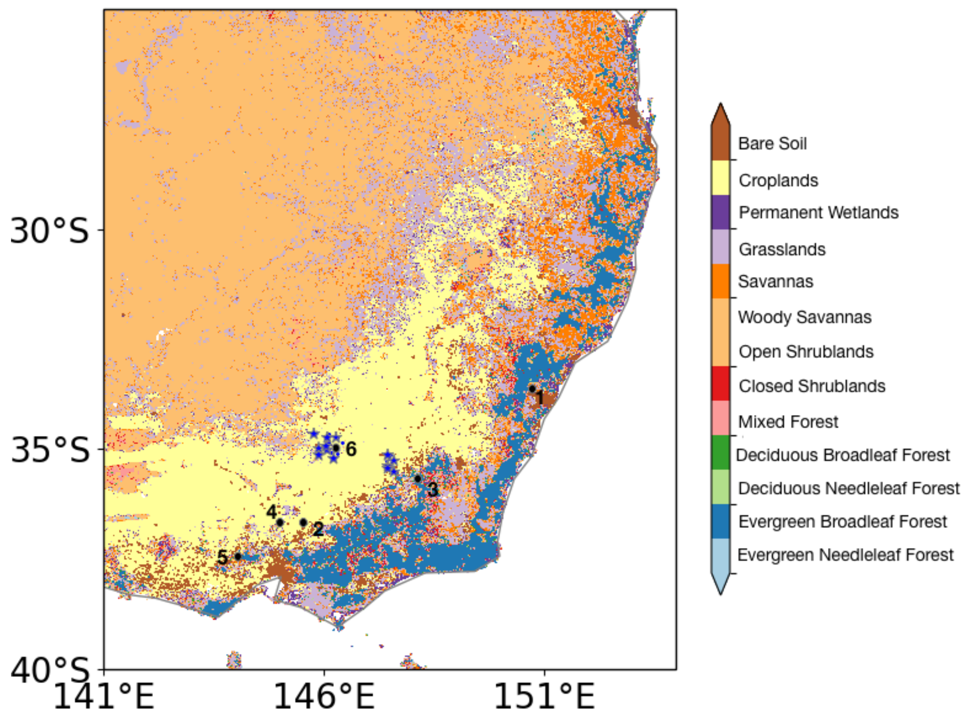

Figure 1. Map of the modeling domain with the MODIS landcover map as the background. The circles represent the locations of the OzFlux stations (1 -Cumberland Plain, 2-Riggs Creek, 3-Tumbarumba, 4-Whroo, 5- Wombat Forest, 6-Yanco). The stars represent the location of the ISMN stations.

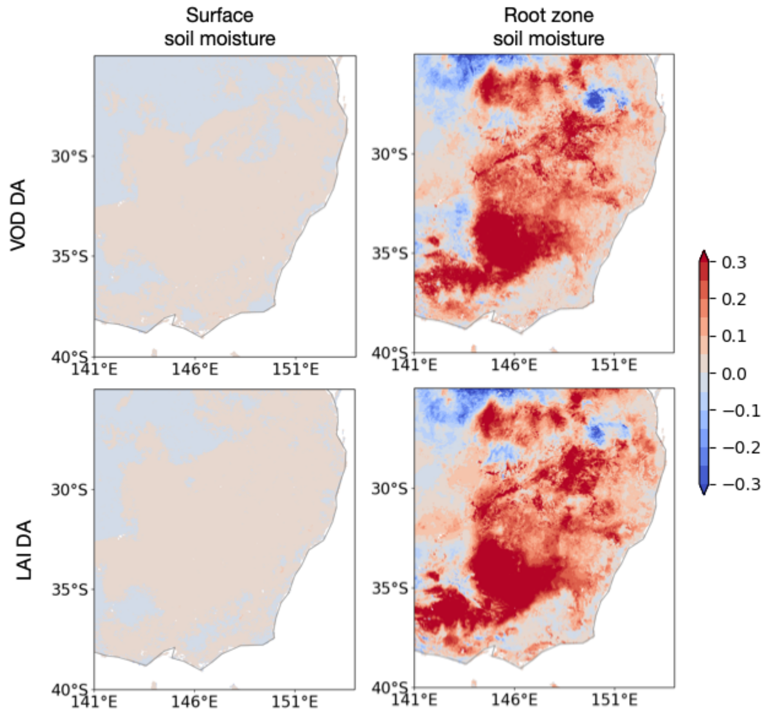

Figure 2. Differences in anomaly R values (during 2015-2020) for surface soil moisture and root zone soil moisture from VOD (top row) and LAI assimilation (bottom row) relative to the OL integration, using the JASMIN soil moisture data as the reference. The warm and cool colors indicate improvements and degradations from DA, respectively.